Journal of Materials Chemistry A

Accepted Manuscript

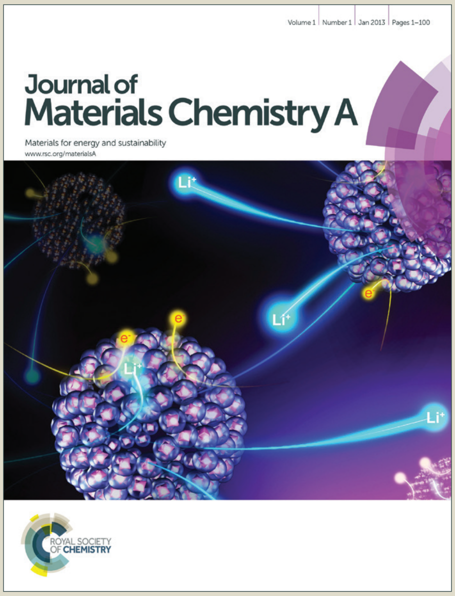

ROYAL SOCIETY OF CHEMISTRY

www.rsc.org/materialsA

Charge transfer processes at the semiconductor/electrolyte interface for solar fuels production: insight from impedance spectroscopy.

Luca Bertoluzzi[a*], Pilar Lopez Varo[b], Juan Antonio Jimenez Tejada[b], Juan Bisquert[a,c]

[a]Grup de Dispositius Fotovoltaics i Optoelectrònics, Departament de Física, Universitat Jaume I, 12071 Castelló, Spain.

[b]Departamento de Electrónica y Tecnología de Computadores, CITIC-UGR, Universidad de Granada, 18071 Granada, Spain

[c]Department of Chemistry, Faculty of Science, King Abdulaziz University, Jeddah, Saudi Arabia

Email: bertoluz@uji.es

Table of content

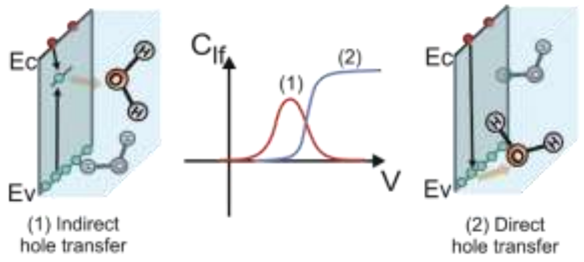

One sentence highlighting the novelty of the work

Low frequency capacitance measurements allow decoupling direct hole transfer from the valence band and indirect hole transfer from surface states.

Abstract

The knowledge of the nature of the charge transfer processes at the semiconductor/electrolyte interface is crucial for the optimization of semiconductors used for solar fuel production. In the literature, there are two types of charge transfer mechanisms: i) direct hole transfer from the valence band and ii) indirect hole transfer via surface states. In this paper we discuss both processes in steady state regime through full drift-diffusion simulations considering the concomitant influence of the electric field and the surface states at the semiconductor/electrolyte interface. We discuss the role of surface state and valence band holes on the photo-anodic current. We subsequently analyze both hole transfer processes in a dynamic regime via the impedance spectroscopy (IS) method. We provide a solid criterion to discriminate both mechanisms and discuss some experimental examples from the literature.

Introduction

The current quest for efficient, clean and cheap energy sources has led to active investigation for alternatives to the classical energy production and storage methods. One promising solution is solar fuel production, which allows transforming solar energy into chemical energy by electrochemical processes with the use of light absorbing semiconductors and catalysts.[1, 2]

However, semiconductors used for solar fuel production must fulfill several conditions which include the low cost of the materials, their earth abundance, absorption in the visible region and long term stability in solution.[3, 4] The sum of all these conditions results in an overall stringent selection criterion, which reduces the panel of available semiconductors to only a few materials. A few set of wide bandgap metal oxides TiO_2,[5] $BiVO_4$,[6] WO_3[7] and Fe_2O_3,[8, 9] which are n type materials, are favored by their stability and suitable energetics for the use as photoanodes for the water oxidation reaction.

Even though these materials are promising, they still display sluggish oxidation kinetics.[10] Two causes have been identified in the literature: i) slow transfer of holes toward the solution and ii) fast electron hole recombination. The first possibility can be justified by the necessity to transfer four holes for water oxidation.[11] The second one can be justified by the presence of a significant density of inner band gap surface states, which is a feature of many oxide semiconductors. Nonetheless, these states may not only act as recombination centers but may also play an important role in the hole transfer process, depending on the physicochemical nature of the semiconductor/electrolyte interface. [12]

In recent years it has been broadly recognized that the functions of light absorption, charge separation and charge transfer can be decoupled forming devices that combine photoactive layer with suitable catalyst and protection layers.[13, 14] Furthermore the high voltage needed for water splitting reaction in combination with the requirement of high photon collection efficiency, recommends the coupling of several middle size bandgap semiconductors to form efficient tandem devices.[15] If a light absorbing semiconductor is supplemented with several layers, it is still needed to understand the operation of such layers in terms of recombination and charge transfer processes.

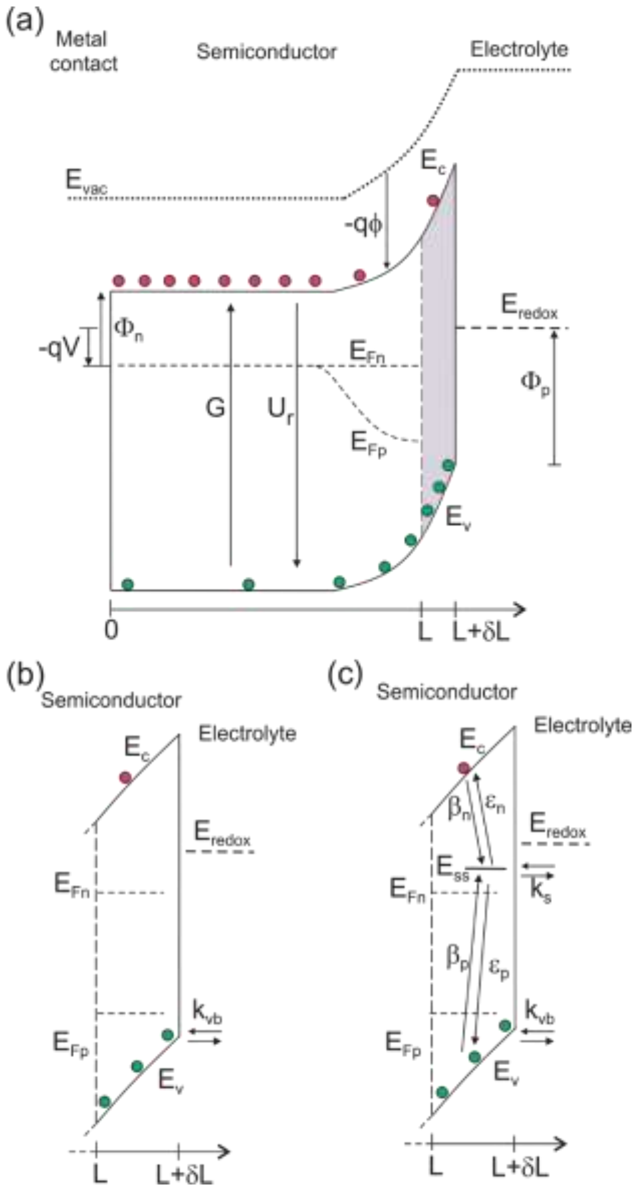

Fig. 1 (a) Energy diagrams for an n type semiconductor of thickness L where electrons and holes are generated at a rate G and recombine at a rate U_r. At the interface of length δL hole transfer to the redox level, E_{redox} can take place (b) directly from the valence band (kinetic constant k_{vb}); and (c) indirectly from the surface states at low bias and directly from the valence band at higher bias. In this latter model, we consider trapping of electrons and holes (β_n and β_p) and detrapping ($\varepsilon_n, \varepsilon_p$) and hole transfer from the surface states (k_s) at the energy level E_{ss}, in competition with direct hole transfer. In these schemes E_c and E_v are the energies of the lower edge of the conduction band and the higher edge of the valence band, respectively. E_{Fn} and E_{Fp} are the quasi Fermi levels, Φ_n and Φ_p the injection barriers of electrons and holes, E_{vac} is the local vacuum level, ϕ is the local electrostatic potential and V is the applied voltage.

In general, for the characterization of the photoinduced oxygen evolution reaction (OER) it is necessary to distinguish two competing types of charge transfer processes at the semiconductor/electrolyte interface, which are summarized in Fig. 1. The first one is a direct hole transfer from the valence band while the second one, which we have recently discussed,[16] is an indirect charge transfer from surface states at low bias and from the valence band at higher bias. This latter process may also represent an intermediate reaction step where photo-generated holes are captured in surface adsorbed species.[17] It should be also pointed out that both types of processes, direct and indirect, may occur at the same time in parallel pathways. This is the case, for example, of semiconductor surface that supports a porous catalyst, when both are in direct contact with the electrolyte.

In order to discriminate between direct and indirect transfer mechanisms, several studies have been performed in dynamic regime.[10, 18, 19] One approach consists on measuring the hole chemical capacitance, which can be achieved by impedance spectroscopy (IS).[20] Such capacitance reflects the variation in carrier concentration in a given storage mode (in this case, either surface states or valence band) when the system undergoes a change in Fermi level. In this paper we show calculations of steady state current through full drift-diffusion simulations and the corresponding IS behavior in dynamic regime and we discuss the two main hole transfer processes proposed in the literature. We provide the main criterion which allows differentiating direct and indirect charge transfer through low frequency capacitance measurements.

Model

Let us first discuss the general framework depicted in Fig. 1a, which underlies both models independently of the charge transfer process. We consider here an n type semiconductor of length L with a rectifying selective contact for holes at the semiconductor/electrolyte interface and an ohmic selective contact for electrons at the metal/semiconductor one. In this configuration, the applied voltage, V , regulates the height of the Schottky barrier seen from the semiconductor at the semiconductor/electrolyte interface. The concentration of electrons at the ohmic electron selective contact is constant and equal to the equilibrium concentration, n_0 . At the interface, whose spatial extension is δL, holes can either oxidize water or recombine. The oxidation reaction is facilitated in reverse bias when the electric field at the depletion region is increased and holes accumulate in this region.

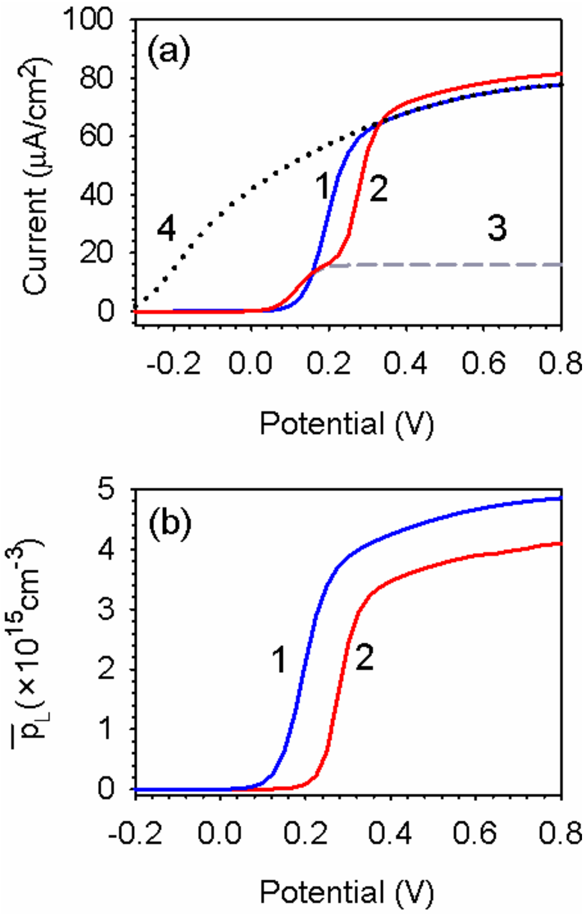

Fig. 2 (a) Full drift diffusion simulations of the current voltage plots when holes are directly transferred from the valence band, as depicted by the model of Fig. 1b (1) and when direct hole transfer competes with indirect charge transfer from the surface states, as shown by the model of Fig. 1c (2). The current associated to hole transfer from the traps, in the framework of this latter model, is represented in grey dashed lines (3). We also indicate the J-V curve for a perfect hole selective contact without surface states (4). (b) Corresponding hole density in the valence band at the semiconductor/electrolyte interface (x = L) as a function of the applied voltage. The parameters used for these simulations are given in Table S1.

We have developed simulations of this model system solving numerically the full set of drift-diffusion equations under illumination detailed in Supporting Information (SI). $\bar{n}$ electrons and $\bar{p}$ holes per unit volume are photo-generated at a rate $G = \alpha\phi_0 \exp(-\alpha x)$, where α is the absorption coefficient and ϕ_0 is the photon flux. They can recombine at a rate $U_r = B(\overline{np} - n_0 p_0)$, B being the recombination constant and p_0 the equilibrium concentrations of holes. In particular the assumption of constant Fermi level of the minority carrier shown in Fig. 1a is not adopted, as the model includes position dependent recombination rate. In Fig. 2 we present the results of current voltage characteristics and the corresponding hole density at the semiconductor/electrolyte interface as a function of the applied voltage for both models presented in Fig. 1. In Fig. 2a, a first plateau is observed at low bias, which corresponds to strong electron-hole recombination and a very small current. When the onset voltage is reached, the barrier height is large and the electric field increases favoring charge separation and reducing recombination. This is when the anodic current rises. Note that this onset voltage strongly depends on the charge transfer process involved in the oxidation reaction. We will discuss this point later on. When the electric field is large enough recombination is completely suppressed, all the photo-generated holes are collected at the interface, and the concentration of holes at the semiconductor/electrolyte interface is constant, as shown in Fig. 2b, independently of the nature of the charge transfer process. For this reason, the current reaches a plateau at higher anodic bias.

Let us now analyze in more detail the influence of the charge transfer process on the current-voltage characteristic. For more clarity we consider all the charge transfer kinetic constants as being independent of the distribution of the donor states in the electrolyte. A more detailed analysis of charge transfer processes in the framework of the Marcus model can be found elsewhere.[21] For direct charge transfer (plot 1 of Fig. 2), the photo-generated holes are directly extracted from the valence band (at a constant rate k_{vb}) and the photocurrent follows the voltage variations of the hole density at the surface. Note that in this case the maximum achievable photo-anodic current can be approximated within the framework of the Reichman model.[22] This approach has been extensively discussed in the literature and for a detailed review of this model we refer the reader to ref.[23]

For indirect charge transfer (plot 2 of Fig. 2), the photo-generated holes are trapped in surface states (hole trapping, β_p, and detrapping, ε_p), at the level E_{ss} with density of surface states per unit volume N_{ss}. The trapped holes can subsequently oxidize water (k_s) or recombine with trapped electrons (electron trapping rate β_n and detrapping rate ε_n). In many semiconductors, these states are distributed within the gap of the semiconductor, and most commonly follow exponential and Gaussian distributions. However, the distribution of surface states does not affect the following discussion and, for the sake of concision, we consider here a mono-energetic density of surface states. In this case the photo-anodic current increases when the surface state assisted recombination decreases, i.e. when the population of trapped electrons drops. When the surface states are being filled with holes, the anodic current reaches a first plateau corresponding to the maximum achievable current from the surface states. This plateau is indicated by the grey dashed lines of Fig. 2a (plot 3). After reaching the first plateau, the photo-anodic current keeps on increasing, along with the hole density in the valence band, which saturates once the surface state assisted recombination has been totally eliminated by the withdrawal of electrons from the surface.

At this point several remarks should be made on the nature of the anodic current depicted in Fig. 2a (plot 2). First of all, there are two contributions to the total anodic current: the surface state current and the one from the valence band. Note that in the case of Fig. 2a (plot 2), the anodic current is higher than the photogenerated current, which shows that photo-generation of holes is not the only process governing the anodic current. In fact it must be pointed out that the current from surface states finds its origin in the removal of the electrons present at equilibrium in these states, either by capture of photogenerated holes (β_p) or by detrapping of electrons from these states to the conduction band (ε_n) when applying an anodic bias. In other words, the anodic current from these states originates not only from photo-generation but also from the applied bias. However the maximum achievable anodic current depends on the recombination kinetics, as suggested by Fig. S1. Secondly, it should be remarked that the onset voltage depends on the electron detrapping (ε_n) and charge transfer (k_s) kinetics.[16] In particular higher charge transfer kinetics may result in a smaller onset voltage in the presence of surface states. It should be emphasized however that this cannot be explained by photo-generation of holes since in this case

Surface states may therefore be an asset for solar fuel production if the kinetics of indirect charge transfer can be enhanced, as suggested by Fig. 2a. It is therefore crucial to identify the origin of the low bias charge transfer process in order to optimize solar fuel production.

Salvador and coworkers[24] have already proposed a criterion in order to discriminate between direct and indirect hole transfer processes in steady state conditions. They demonstrated that the photocurrent depends on illumination as $\alpha\phi_0$ for direct charge transfer and as $\sqrt{\alpha\phi_0}$ for indirect charge transfer. However, this statement holds only under low recombination conditions. For a more general approach, a dynamic study is necessary. A very popular method is IS, which allows decoupling faradic processes (in this case charge transfer and recombination processes) by activating capacitive processes via a small frequency dependent perturbation of voltage. IS measurements are usually represented in terms of complex plane plots where the imaginary part of the measured impedance is represented as a function of its real part. In this representation, the resulting patterns are semicircles which can be analyzed with the use of equivalent electrical circuits (EC). For each semicircle, one capacitance and one resistance values can be extracted. For the case of fuel production with wide band gap semiconductors, a maximum of two semicircles is generally observed, depending on the applied voltage. As a result, two resistance and capacitance values can be obtained from such measurements. The extraction of these latter elements and the adequate physical interpretation of the model relies first of all on the proper choice of EC.

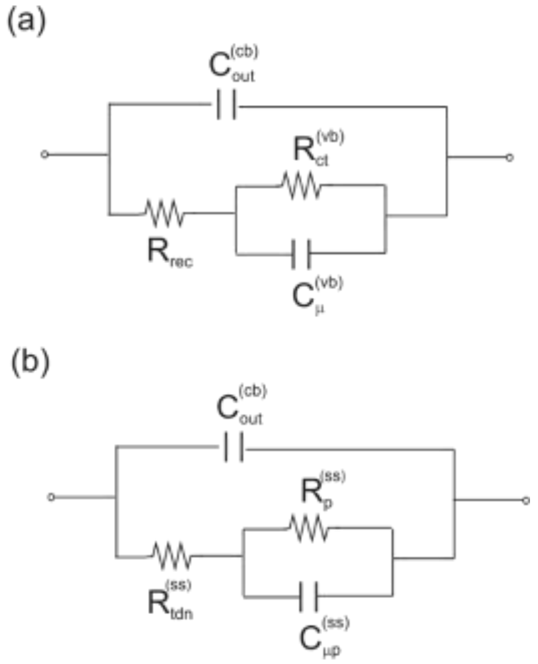

Fig. 3 Equivalent circuit (EC) obtained from a small ac perturbation for (a) the direct hole transfer model of Fig. 1b and (b) the indirect hole transfer model of Fig. 1c. In these circuits $C_{out}^{(cb)}$ is the semiconductor capacitance, $C_{\mu}^{(vb)}$ is the valence band equilibrium chemical capacitance, $C_{\mu p}^{(ss)}$ is the surface state chemical capacitance, R_{rec} is the band to band recombination resistance, $R_{ct}^{(vb)}$ is the hole transfer resistance from the valence band, $R_{tdn}^{(ss)}$ is the trapping/detrapping resistance of electrons from the conduction band and $R_{p}^{(ss)}$ is the hole transfer resistance from the surface states.

In view of the previous considerations we shall now discuss the ECs presented in Fig. 3 for both hole transfer models. Note that for the sake of clarity, we consider in the following only the processes at the interface and neglect the transport limitations and all quantities are therefore considered constant. Moreover, since we consider the low bias regime, we can neglect charge transfer from the valence band in the case of Fig. 1c. Under these assumptions, the EC for the systems presented in Fig. 1b and c are given in Fig. 3a and b. More details on the calculation of such ECs are given in SI. The EC of Fig. 3a is a simplification of the general transmission line model presented in a recent publication[25] with an additional charge transfer resistance for holes from the valence band and without the dielectric relaxation channel. From this EC, we can extract values for two capacitances and resistances, which are associated to the conduction and valence band carriers. The EC of Fig. 3b corresponds to the classical EC for the trapping/detrapping and charge transfer of a single type of carrier.[26, 27] We have already discussed in detail this EC with the additional contribution of valence band holes.[16] In this configuration, we predicted the theoretical possibility of three semicircles in the complex plane. However, in the present discussion we omit the direct hole transfer from the valence band which takes place at higher voltages and the low frequency arc corresponding to the valence band hole transfer disappears. Then the circuit of Fig. 3b allows extracting values for two resistances and two capacitances, which are associated with the conduction band and surface states. Note that in this configuration, it is impossible to probe the hole population and consequently extract the recombination resistance associated to electron hole recombination in the traps. For the latter purpose, other techniques are needed, such as Intensity Modulated Photocurrent Spectroscopy (IMPS),[28] where light intensity modulations allow to directly vary and probe the hole concentration in the valence band.

Interestingly, both ECs presented in Fig. 3 are identical but the physical nature of the electrical elements is different. Of particular interest are the low frequency capacitances, which give valuable information on the storage mode of the photo-generated holes which are involved in the water photo-oxidation. For the EC of Fig. 3a, the low frequency capacitance is associated with valence band holes with concentration $\bar{p}_L$ at the semiconductor/electrolyte interface:

$$C_{\mu}^{(vb)} = \frac{q^2 L}{k_B T}\bar{p}_L \tag{1}$$

For Figure 3b, the low frequency capacitance is associated to holes in the surface states and it is written as:

$$C_{\mu p}^{ss}=\frac{q^2L}{k_BT}B_{ss}^{-1}\bar{f}(1-\bar{f})N_{ss} \tag{2}$$

Where $\bar{f}$ is the steady state electron occupation probability of the surface states at the semiconductor/electrolyte interface ($x = L$) and B_{ss} is a factor such that $0 < B_{ss} \leq 1$. $\bar{f}$ and B_{ss} are defined by:

$$\bar{f}=\frac{\beta_n\bar{n}_L+k_s f_0-GL/(N_{ss}\delta L)}{\beta_n\bar{n}_L+\varepsilon_n+k_s} \tag{3}$$

$$B_{ss}=\frac{\delta L}{L}\left(1+\frac{\varepsilon_n}{\beta_n\bar{n}_L}\right)\bar{f} \tag{4}$$

In eqn (3) and (4), $\bar{n}_L$ is the steady state density of electrons at the interface semiconductor/electrolyte.

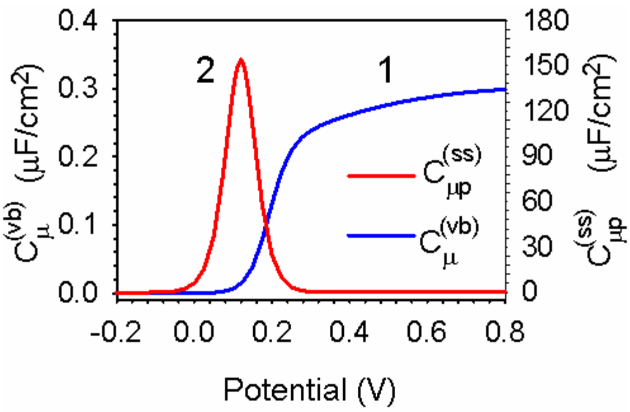

Fig. 4 Low frequency capacitances for the direct charge transfer model of Fig. 1b (1) and the indirect charge transfer model of Fig. 1c (2). The former one is associated to hole storage in the valence band while the latter one is related to hole accumulation in surface states. The steady state electrical magnitudes and parameters involved in the calculations of these capacitances (eqn (1)−(4)) are the ones obtained from the full drift-diffusion simulations of Fig. 2.

Both capacitances are represented as a function of voltage in Fig. 4. The voltage dependence for both types of capacitance is clearly different. In fact, the surface state capacitance reaches a peak which marks the transition between occupied (filled with electrons) and unoccupied (filled with holes) surface states. On the contrary, the valence band chemical capacitance is directly proportional to the concentration of holes in the valence band and reaches saturation at higher voltages, as suggested by Fig. 2b. Thus, low frequency capacitance measurements are a powerful tool for the distinction between direct and indirect charge transfer.

Discussion

The presence of surface states at the semiconductor/electrolyte interface not only depends on the morphology of the semiconductor surface but also on the nature and composition of the electrolyte. TiO_2 is certainly one of the most popular examples that can be found in the literature.[29] In particular nano-structured TiO_2 is featured by two types of defects:[30, 31] i) an exponential tail of defects which arises from the under-coordinated four-fold coordinated surface Ti[32] and ii) a mono-energetic level of Ti interstitials/Oxygen vacancies that are due to uncoordinated Ti surface ions.[33] This latter type of defects evolves as OH radicals under illumination in aqueous electrolyte and can be involved in the photogeneration of H_2O_2, which in turn adsorbs on TiO_2 surface and acts as a temporary surface state.[17, 34] Recently, Reckers et al. showed that in addition to the deposition method, synchrotron exposure can also strongly influence the density of deep and shallow inner band gap states.[35]

In the case of α-Fe_2O_3 (hematite) a clear capacitive peak has been observed, which unveiled charge transfer from the surface states in aqueous solution.[12] These states have the particularity that they can only be observed at anodic bias and under illumination.[36] In addition, hematite surface states are strongly dependent on the nature of the electrolyte. A recent study has shown that in presence of water, methanol or acetonitrile, the distribution of hematite surface states drastically change.[9] Moreover, Iandolo and Hellman[37] demonstrated an anodic shift of the surface state capacitive peak with pH. These authors analyzed the nature of the surface states involved in the capacitive response with DFT calculations. They showed that Fe_2O_3 surface is populated with two types of terminations: –O and –OH, which both act as surface states. –OH induced states are close to the middle of the semiconductor band gap and act as recombination centers at low bias, while –O terminations are close to the valence band and allow hole transfer at higher bias. Both states where observed by impedance spectroscopy and cyclic voltammetry by Klahr and Hamann[38] for hematite in aqueous electrolyte. The same group concomitantly showed that the surface states identified as recombination centers could be selectively removed by using atomic layer deposition (ALD) and annealing hematite at 800ºC.[39] Chou and coworkers[40] have observed that hole transfer from hematite surface states depends on the deposition method. In particular, by measuring the low frequency capacitance associated to surface states, they have shown that hole transfer from these states is more favorable for oxidation of Fe than for anodic electrodeposition. In the case of hematite obtained by vapor deposition in a 1 M NaOH, a 580 nm spectral signal has by observed by Durant's group[41] by Transient Absorption Spectroscopy (TAS). They ascribed this spectral feature to a hole transition between the valence band and localized states, which were identified as iron-oxygen vacancy complexes. They also observed long lived holes at higher applied bias (> 0.8 V vs RHE) and confirmed these results by IS[18] however these results may be influenced by parasitic faradic processes at such large bias.

Doyle and coworkers[42] obtained similar results as the one of hematite for the pH dependence of hydrous iron oxide. Through IS measurements, they observed a direct pH dependence of the low frequency capacitance. For very basic aqueous solution (concentration of NaOH superior to 1 mol/L), they observed a clear capacitive peak associated to surface states, which they identified as Fe=O intermediaries. On the contrary for lower concentrations of NaOH (inferior to 0.5 mol/L), they measured a capacitance similar to the valence band capacitance displayed in Fig. 4 (plot 1).

Finally, the presence of a hole scavenger or an over-layer for catalysis or passivation purposes strongly influences the nature of the hole transfer process. In presence of hole scavengers such as $[Fe(CN)_6]^{3-/4-}$,[43] H_2O_2[44] or CH_3OH,[9] hematite does not present the capacitive peak behavior induced by surface states and direct hole transfer from the valence band is certainly occurring. In this case, the IS pattern is a single semicircle that is associated to the semiconductor capacitance ($C_{out}^{(cb)}$ in the ECs of Fig. 3), which allows obtaining the Mott-Schottky plot of the material. It is however unfeasible to observe with IS the low frequency valence band capacitance ($C_{\mu}^{(vb)}$) for such large band gap materials. In presence of an over layer such as Co-Pi,[19] IrO_x[45] on hematite, it has been observed that the hole transfer resistance is enhanced. In some cases, the oxide layer increases hole recombination, as in the case of MnO_x.[46] In addition, such layers generally introduce a capacitance which hides the surface state capacitance. In this case, the over layer allow accumulating holes and reduce surface recombination.[35] However, in this situation it is a complex task to ascribe the diminution of recombination to an increase of the charge transfer kinetics only or to a concomitant passivation of the surface states. As stated by Sivula, the term catalyzer takes a whole new dimension for semiconductors.[47] An example is the study performed by Riha and coworkers who have observed a significant improvement of the onset voltage and photo-current when depositing by ALD an ultrathin layer of $Co(OH)_2/Co_3O_4$ on top of hematite.[48] Their EIS analysis revealed a decrease in surface state capacitance and charge transfer resistance. In this case the passivating layer allowed improving the kinetics of hole transfer as well as decreasing the density of surface states.

Conclusion

Two hole transfer processes have been discussed for the oxidation reaction at the interface semiconductor/electrolyte. The first one is a direct hole transfer from the valence band. The second one is an indirect charge transfer from surface states. We have performed full drift-diffusion simulations and have shown that independently of the charge transfer process the hole concentration at the semiconductor/electrolyte must saturate at higher anodic bias, and so does the anodic current. In addition, we have shown that surface states may be an asset for fuel production since good charge transfer kinetics from these states can give lower onset voltages as well as higher anodic current. In dynamic regime, we have shown that both charge transfer processes can be modelled by the same EC when applying the IS method. However the nature and voltage behavior of the electrical elements of both ECs are different. In particular, the low frequency capacitance associated to the valence band holes for the direct charge transfer model shows a saturation at higher voltage. On the contrary, the one related to the surface state holes for the indirect charge transfer model displays a peak behavior with voltage. However the capacitive behavior is strongly dependent on the nature of the semiconductor/electrolyte interface.

Acknowledgements

The research leading to these results has received funding from the European Union Seventh Framework Program [FP7/2007-2013] under grant agreement 316494 and MINECO of Spain under project MAT2013-47192-C3-1-R. This work was also supported by Ministerio de Educación y Ciencia under research Grant FPU12/02712, and under research Project from MINECO, TEC2013-47283-R

References

1. A. J. Nozik, *Annu. Rev. Phys. Chem.* , 1978, **29**, 189.
2. M. A. Butler and D. S. Ginley, *J. Mater. Sci.*, 1980, **15**, 1-19.
3. J. Bolts and M. Wrighton, *J. Phys. Chem.*, 1976, **80**, 2641-2645.
4. M. G. Walter, E. L. Warren, J. R. McKone, S. W. Boettcher, Q. Mi, E. A. Santori and N. S. Lewis, *Chem. Rev.*, 2010, **110**, 6446-6473.
5. A. Fujishima and K. Honda, *Nature*, 1972, **238**, 37-38.
6. Y. Zhang, Y. Guo, H. Duan, H. Li, C. Sun and H. Liu, *Phys. Chem. Chem. Phys.*, 2014, **16**, 24519-24526.
7. C. Santato, M. Ulmann and J. Augustynski, *J. Phys. Chem. B*, 2001, **105**, 936-940.
8. H. K. John and Karl W. Frese, Jr., *J. Electrochem. Soc* 1978, **125**, 709-714.
9. B. Klahr, S. Gimenez, O. Zandi, F. Fabregat-Santiago and T. Hamann, *ACS applied materials & interfaces*, 2015, **7**, 7653-7660.
10. L. M. Peter, K. G. U. Wijayantha and A. A. Tahir, *Farad. Discuss.*, 2012, **155**, 309-322.
11. J. Tang, J. R. Durrant and D. R. Klug, *J. Am. Chem. Soc.*, 2008, **130**, 13885-13891.
12. B. Klahr, S. Gimenez, F. Fabregat-Santiago, T. Hamann and J. Bisquert, *J. Am. Chem. Soc.*, 2012, **134**, 4294-4302.
13. K. Maeda and K. Domen, *J. Phys. Chem. Lett.*, 2010, **1**, 2655-2661.
14. S. Y. Reece, J. A. Hamel, K. Sung, T. D. Jarvi, A. J. Esswein, J. J. H. Pijpers and D. G. Nocera, *Science*, 2011, **334**, 645-648.
15. Y. Tachibana, L. Vayssieres and J. R. Durrant, *Nat Photon*, 2012, **6**, 511-518.
16. L. Bertoluzzi and J. Bisquert, *J. Phys. Chem. Lett.*, 2012, **3**, 2517-2522.
17. P. Salvador and C. Gutierrez, *J. Phys. Chem.*, 1984, **88**, 3696-3698.
18. F. Le Formal, S. R. Pendlebury, M. Cornuz, S. D. Tilley, M. Grätzel and J. R. Durrant, *J. Am. Chem. Soc.*, 2014, **136**, 2564-2574.
19. B. Klahr, S. Gimenez, F. Fabregat-Santiago, J. Bisquert and T. W. Hamann, *J. Am. Chem. Soc.*, 2012, **134**, 16693-16700.
20. J. Bisquert, *Phys. Chem. Chem. Phys.*, 2003, **5**, 5360-5364.
21. J. Bisquert and R. Marcus, in *Multiscale Modelling of Organic and Hybrid Photovoltaics*, eds. D. Beljonne and J. Cornil, Springer Berlin Heidelberg, 2014, vol. 352, ch. 471, pp. 325-395.
22. J. Reichman, *Appl. Phys. Lett.*, 1980, **36**, 574-577.
23. P. Cendula, S. D. Tilley, S. Gimenez, J. Bisquert, M. Schmid, M. Grätzel and J. O. Schumacher, *J. Phys. Chem. C*, 2014, **118**, 29599-29607.
24. I. Mora-Seró, T. Lana-Villarreal, J. Bisquert, A. Pitarch, R. Gómez and P. Salvador, *J. Phys. Chem. B*, 2005, **109**, 3371-3380.
25. J. Bisquert, L. Bertoluzzi, I. Mora-Sero and G. Garcia-Belmonte, *J. Phys. Chem. C*, 2014, **118**, 18983-18991.
26. J. Bisquert, *J. Electroanal. Chem.*, 2010, **646**, 43–51.
27. Z. Hens, *J. Phys. Chem. B*, 1999, **103**, 122-129.
28. E. A. Ponomarev and L. M. Peter, *J. Electroanal. Chem.*, 1995, **397**, 45-52.
29. Y. Nakato, A. Tsumura and H. Tsubomura, *J. Phys. Chem.*, 1983, **87**, 2402-2405.
30. K. Schwanitz, U. Weiler, R. Hunger, T. Mayer and W. Jaegermann, *J. Phys. Chem. C*, 2006, **111**, 849-854.
31. L. Bertoluzzi, I. Herraiz-Cardona, R. Gottesman, A. Zaban and J. Bisquert, *J. Phys. Chem. Lett.*, 2014, **5**, 689-694.
32. D. Monroe and M. A. Kastner, *Phys. Rev. B*, 1986, **33**, 8881-8884.
33. F. Nunzi, E. Mosconi, L. Storchi, E. Ronca, A. Selloni, M. Gratzel and F. De Angelis, *Energy Environ. Sci.*, 2013, **6**, 1221-1229.
34. C. Fàbrega, D. Monllor-Satoca, S. Ampudia, A. Parra, T. Andreu and J. R. Morante, *J. Phys. Chem. C*, 2013, **117**, 20517-20524.
35. M. Risch, F. Ringleb, M. Kohlhoff, P. Bogdanoff, P. Chernev, I. Zaharieva and H. Dau, *Energy Environ. Sci.*, 2015, **8**, 661-674.
36. L. Bertoluzzi, L. Badia-Bou, F. Fabregat-Santiago, S. Gimenez and J. Bisquert, *J. Phys. Chem. Lett.*, 2013, **4**, 1334-1339.

37. B. Iandolo and A. Hellman, *Angew. Chem. Int. Edit.*, 2014, **53**, 13404-13408.
38. B. Klahr and T. Hamann, *J. Phys. Chem. C*, 2014, **118**, 10393-10399.
39. O. Zandi and T. W. Hamann, *J. Phys. Chem. Lett.*, 2014, **5**, 1522-1526.
40. J.-C. Chou, S.-A. Lin, C.-Y. Lee and J.-Y. Gan, *J. Mater. Chem. A*, 2013, **1**, 5908-5914.
41. M. Barroso, S. R. Pendlebury, A. J. Cowan and J. R. Durrant, *Chem. Sci.*, 2013, **4**, 2724-2734.
42. R. L. Doyle and M. E. G. Lyons, *Phys. Chem. Chem. Phys.*, 2013, **15**, 5224-5237.
43. B. Klahr, S. Gimenez, F. Fabregat-Santiago, J. Bisquert and T. W. Hamann, *Energy Environ. Sci.*, 2012, **5**, 7626-7636.
44. H. Dotan, K. Sivula, M. Gratzel, A. Rothschild and S. C. Warren, *Energy Environ. Sci.*, 2011, **4**, 958-964.
45. L. Badia-Bou, E. Mas-Marza, P. Rodenas, E. M. Barea, F. Fabregat-Santiago, S. Gimenez, E. Peris and J. Bisquert, *The Journal of Physical Chemistry C*, 2013, **117**, 3826-3833.
46. X. Yang, C. Du, R. Liu, J. Xie and D. Wang, *J. Catal.*, 2013, **304**, 86-91.
47. K. Sivula, *J. Phys. Chem. Lett.*, 2013, **4**, 1624-1633.
48. S. C. Riha, B. M. Klahr, E. C. Tyo, S. Seifert, S. Vajda, M. J. Pellin, T. W. Hamann and A. B. F. Martinson, *ACS Nano*, 2013, **7**, 2396-2405.